Materials LAB

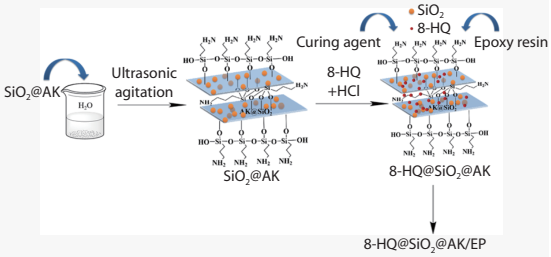
RESEARCH ARTICLE

Materials Lab 2024, 3, 230018

Preparation and anti-corrosion properties of 8-HQ@SiO_2@AK/EP composite materials

Ju Li[1], Renzhe Jin[1], Mengyuan He[1], Qiang Zhao[1], Zhengyu Wei[1], Panfei Sun[1], Dehai Ping[1], Xiaomei Yu[1] and Songjie Li[1,2*]

Epoxy coatings are popular due to their strong adhesion, low cost, and superior thermal and electrical insulation. Unfortunately, surface defects in epoxy resin lead to surface cracks, limiting the long-term use of epoxy resin coatings in humid marine environments. In this study, modified kaolin (Kaolin) was added to an epoxy resin (EP) to enhance its corrosion resistance, and a silane coupling agent 3-aminopropyltriethoxysilane (APTES), tetraethyl orthosilicate (TEOS), and 8-hydroxyquinoline (8-HQ) were chosen as modifiers. This resulted in the composite 8-hydroxyquinoline/silica/amino kaolin (8-HQ@SiO_2@AK), and the structural makeup, loading, hydrophobic characteristics, surface roughness, and corrosion resistance of 8-HQ@SiO_2@AK and 8-hydroxyquinoline/silica/amino kaolin/epoxy resin composite coating (8-HQ@SiO_2@AK/EP) was investigated. Based on these findings, the maximum contact angle of the hydrophobic composite coating was 88°, its roughness Ra was 3.09 nm, and the hardness and adhesion were unaltered compared to silica-modified kaolin/epoxy composite coatings (SiO_2@AK/EP). The impedance modulus $|Z|_{0.01\ Hz}$ of the composite was $3.662\times10^9\ \Omega \cdot cm^2$ after 30 days of immersion, which indicated significantly enhanced corrosion resistance.



Metal corrosion wastes important energy and resources, contributes to environmental pollution, and even results in catastrophic accidents in the industrial sector and society at large[1, 2]. Every year, considerable metal machinery, parts, and other materials are lost to the national economy owing to corrosion[3]. More money is lost every year due to metal corrosion than is lost as a result of all fires, floods, and other natural catastrophes combined. Several offshore engineering tools are utilized in the marine environment for extended periods of time while immersed in seawater, including offshore oil platforms, cross-sea bridges, deep-sea exploration equipment, ships, and other metal structures. Seawater is a corrosive medium that attacks the metal elements in offshore equipment and causes pitting, hydrogen embrittlement, stress corrosion fractures, fatigue corrosion, and major health and financial losses[4]. Marine corrosion protection has recently received considerable attention, and while anti-corrosion technology is also continually evolving[5-7], it is still far from satisfying industrial demand. The development of anti-corrosion technology as well as studies and preparation of high-performance materials have become crucial issues for marine engineering.

Epoxy resin (EP) is a thermosetting polymer that is frequently used in primers because of its electrical insulation, chemical resistance, and thermal stability. It has excellent alkali and solvent resistance, and the aliphatic hydroxyl, ether, and epoxy groups and other active groups strongly adhere to metal surfaces. There are several flaws, though. Epoxy coatings need to be adjusted since they have poor resistance to water and outside weather, are permeable to corrosive media such as water and oxygen and are poor barriers[8-10]. The corrosion resistance and protective capabilities of epoxy resins are significantly enhanced by the laminar structure of nano kaolinite and its poor ion exchange capacity, which effectively increases the lengths of the diffusion channels for the corrosive medium[11]. The silane coupling agent APTES is used to replace some of the hydroxyl groups in the silicate to improve the dispersion since kaolin has a tendency to agglomerate in the resin. Coatings frequently contain nanomaterials. Due to their small particle sizes and high aspect ratios, inorganic nanoparticles can fill the pores of organic coatings and enhance the coating performance. Nanoparticles are added to epoxy resins to prepare a corrosion-inhibiting medium or provide barrier protection[12]. Nanomaterials such as 8-HQ[13], SiO_2[14, 15], Al_2O_3[16], Cr_2O_3[17], and ZnO[18] are frequently employed. In this study, SiO_2 was added to the surface of the 2D material APTES@Kaolin and loaded with the

[1] *School of Chemical Engineering, Zhengzhou University, 100 Science Avenue, Zhengzhou 450001, China*

[2] *Engineering Research Center of Advanced Functional Material Manufacturing of Ministry of Education, Zhengzhou University, 100 Science Avenue, Zhengzhou 450001, China*

* Corresponding author, E-mail: songjie@zzu.edu.cn

Received 6 April 2023; Accepted 18 May 2023; Published online

© 2024 The Author(s). *Materials Lab* published by Lab Academic Press

DOI: 10.54227/mlab.20230018

small molecule corrosion inhibitor 8-HQ to create a composite 8-hydroxyquinoline/silica/aminated kaolin (8-HQ@SiO_2@AK). The effects of temperature, time, and solution pH on the reaction products were examined. Using FTIR and other characterization techniques, the material composition was examined, and UV testing was used to calculate the corrosion inhibitor loading. To increase the hydrophobicity, hardness, adhesion, and electrochemical corrosion resistance of the composite coatings, the composites were also added to epoxy resin coatings.

Materials and methods

Preparation of 8-HQ@SiO_2@AK composites

Two hundred millilitres of aqueous ethanol was mixed with 450 mg of kaolin for 30 minutes before the addition of 3-aminopropyltriethoxysilane (APTES, AR). The sample was heated and stirred at 70 °C for 5 hours, cooled, and then washed three times with water and three times with ethanol before drying at 60 °C for 12 hours. The composite APTES@kaolin (AK) resulted.

100 mg of AK was dispersed into 100 ml of deionized water and sonicated for 1 h. After adjusting the solution to pH 12 with 1 mol·L^{-1} NaOH, tetraethyl orthosilicate (TEOS, AR) was added and heated in an oil bath at 80 °C for 5 h. To create the composite SiO_2@AK, the samples were cooled, filtered, and washed three times each with ethanol and water and then dried at 60 °C for 12 hours.

After sonication in 100 mL of deionized water for one hour, 50 mg of SiO_2@AK was added to the 8-hydroxyquinoline (8-HQ). A 1 mol L^{-1} hydrochloride solution was used to adjust the pH, and the mixture was heated and agitated for one hour. The reaction was conducted for 12 hours at 80 °C in an oil bath. The samples were filtered, cooled, and washed three times each with water and ethanol and then tested with an $AgNO_3$ solution to see if all of the Cl^- had been eliminated. The composite 8-HQ@SiO_2@AK was dried for 12 hours at 60 °C.

Preparation of the 8-HQ@SiO_2@AK/EP composite coating

The experimental substrate comprised Q235 mild steel, and the specimen dimensions were 70 mm × 40 mm × 2 mm. The steel plates were cleaned by ultrasonication in anhydrous ethanol after they were sanded with 100, 400, and 800 grit sandpaper. 18 mg of 8-HQ@SiO_2@AK was weighed, a diluent was added, and the mixture was stirred for 30 minutes. To prepare the composite coating 8-HQ@SiO_2@AK/EP, epoxy resin and a curing agent were added and mixed to remove air bubbles. A 110 ± 10 μm thick layer of the composite coating was placed on the prepared steel plate and allowed to cure for five days at room temperature.

Testing and characterization

Atomic force microscopy (AFM, HITACHI SU5000$^+$) and scanning electron microscopy were used to examine the microscopic morphology of the composite coating (AFM, Bruker Dimension com). The structural makeup of the composite coatings was identified with X-ray diffraction (XRD, BruckerD8 Advance). Using a Fourier transform infrared spectrometer (FTIR, Bruker), the Fourier transform infrared (FTIR) spectra were captured in the 400–4000 cm^{-1} wavenumber range. A PARSTAT MC electrochemical workstation was used to generate polarization curves and perform AC impedance tests (EIS). A three-electrode system was used for AC impedance tests (EIS); the working electrode was attached to a piece of Q235 carbon steel that had been coated with the composite coating, while the reference electrode was a polymeric electrode and the counter electrode was a graphite electrode. Atomic force microscopy (AFM, HITACHI SU5000$^+$) and scanning electron microscopy were used to examine the microscopic morphology of the composite coating (AFM, Bruker Dimension com). The composite pore size distribution, specific surface area, and pore volume were all determined with an ASAP 2460 BET-specific surface area analyser (Mike, USA). The test gas utilized was N_2, and the relative pressure ratio (P/P_0) was 0 to 1. The release profile of the corrosion inhibitor was evaluated in a NaCl solution with a UV-2600 UV tester (Shimadzu, Japan) over the wavelength range 195 cm^{-1} – 260 cm^{-1}. OCA data physics was used to evaluate the hydrophobicity of the composite coating, and a 20-contact angle tester was used. Cold monochromatic LEDs with adjustable brightness were employed as the light sources.

Results and discussion

Characterization and analysis of 8-HQ@SiO_2@AK

The FTIR spectra of 8-HQ@SiO_2@AK samples produced with various reaction temperatures, periods, and pH levels are shown in Fig. 1. As demonstrated in Fig. 1a, 8-HQ@SiO_2@AK exhibited a peak in the 1250–1600 cm^{-1} wavelength region, which was associated with the C–O, C–N, and C=N stretching vibrations of the small organic molecule 8-HQ[19,20]. The strong –CH_3 peak in 2750 cm^{-1} to 3250 cm^{-1} wavelength range indicated successful loading of the 8-HQ into SiO_2@AK. The characteristic peaks of 8-HQ changed from double peaks to single peaks in the composite product and were observed at 1250 cm^{-1} to 1500 cm^{-1}, as seen in Fig. 1b-d; this resulted from the increased reaction time and reaction temperature and changes in the acidity and alkalinity of the solution, which may have disrupted some of the structure of 8-HQ and caused dissolution. The reaction byproducts were subjected to XRD analyses to determine the material structure.

The XRD data for 8-HQ@SiO_2@AK samples made under various reaction conditions are shown in Fig. 2. Fig. 2a shows that the XRD curves for 8-HQ@SiO_2@AK and APTES@Kaolin were comparable, and the intensity of the distinctive Kaolin peak was stronger than that of SiO_2@AK. This might have resulted from a reaction of the organic substance with acid or the removal of the silica gel from the surface of the 2D material. The XRD plots for 8-HQ@SiO_2@AK samples produced at various pH values, reaction times, and temperatures are shown in Fig. 2b-d. Changes in the reaction temperature yielded partial reaction at 80 °C but little change for the other reaction temperatures. Changes in the reaction time had no discernible effect on the XRD data, which may have occurred because a high or low H^+ concentration in the solution would limit the extent of the reaction with the organic matter on the surface of the 2D material.

The UV spectra for 8-HQ@SiO_2@AK samples produced with various reaction temperatures, periods, and pH levels are

DOI: 10.54227/mlab.20230018

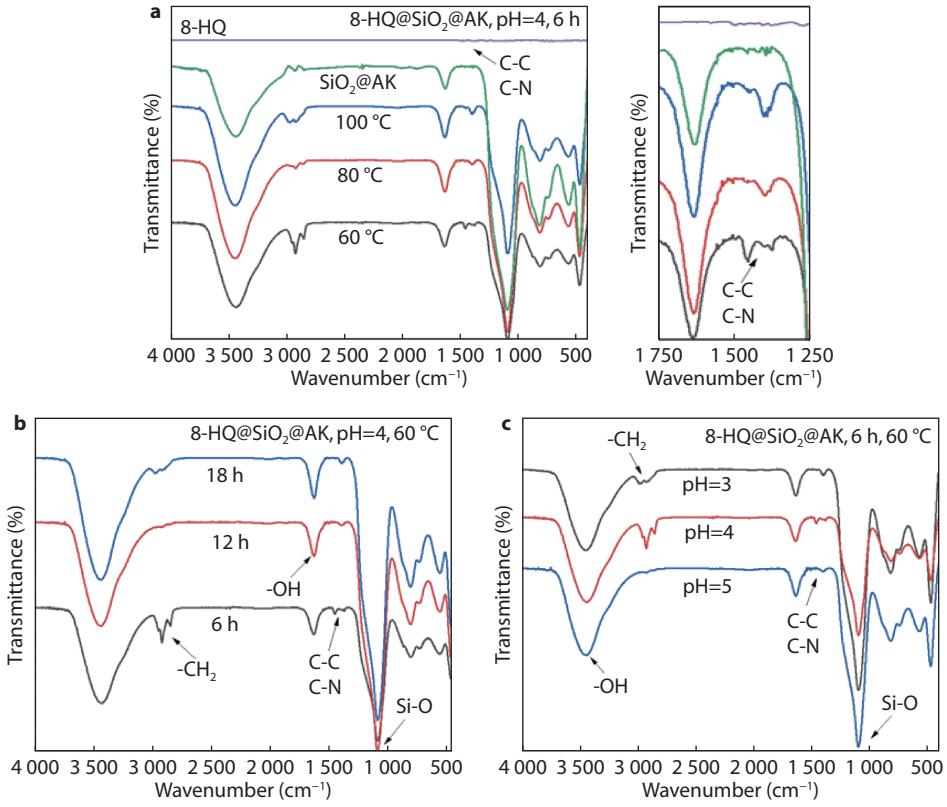


Fig. 1 FTIR diagrams of prepared 8-HQ @SiO_2@AK in different conditions: **a** different reaction temperature; **b** different reactant time and **c** different reaction pH.

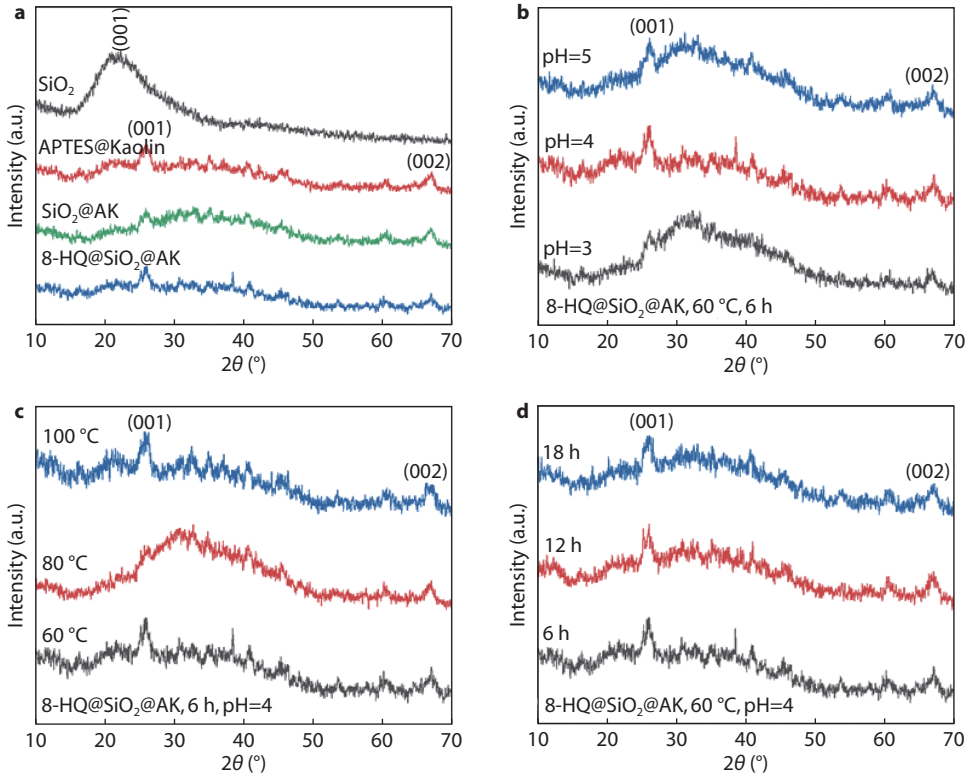


Fig. 2 XRD diagrams of 8-HQ@SiO_2@AK prepared in different conditions: **a** comparison chart before and after modification; **b** different reaction pH; **c** different reaction time and **d** different reactant temperature.

DOI: 10.54227/mlab.20230018

shown in Fig. 3a–i. The figures show that the absorption of 8-HQ steadily increased over the course of 24 hours. Several 8-HQ loading sites and loading intensities seen for various reaction conditions resulted in different release rate patterns. The findings indicate that while the reaction time had limited impact on loading, the reaction temperature and pH had substantial impacts. A pH of 3, a reaction temperature of 80 °C, and a reaction duration of 6 h were selected to prepare samples for additional performance evaluation.

The SEM images of the SiO_2@AK and 8-HQ@SiO_2@AK composite surfaces are shown in Fig. 4a-b and c-d, respectively. The composites both comprised two-dimensional materials with small surface holes and nanoparticles of various sizes adhering to the surface. This indicated that the addition of 8-HQ did not alter the original structure and maintained the dispersion of the 2D nanomaterial composite in the epoxy resin. The morphological changes of the composites after the modification were negligible, and no obvious agglomeration appeared.

Thermogravimetric plots for the SiO_2@AK and 8-HQ@SiO_2@AK composites are shown in Fig. 5. The TG and DTG curves for 8-HQ@SiO_2@AK are shown in Fig. 5b. A small weight loss occurred between 96 °C and 524 °C due to acid washing of the silica gel in the material during the reaction; this removed many hydroxyl groups and bound water and some of the adsorbed 8-HQ, which replaced some of the amino groups and was inserted between layers of kaolin clay[21]. The mass loss occurring below 96 °C was primarily attributed to adsorption. The covalent bonds at the material edges were broken, the surface silanes were lost, and the weakly adsorbed and reactive 8-HQ was decomposed. The amount of surface-adsorbed silane lost was substantially less than that of SiO_2@AK, which suggested that 8-HQ successfully replaced the amino groups. According to the FTIR data, additional heating dehydroxylated the composite.

The isothermal adsorption-desorption curves and pore size distributions of the composite are shown in Fig. 6. As seen in Fig. 6a, the composite still exhibited a loose lamellar particle structure with slit-like pores because the adsorption and desorption curves of the 8-HQ@SiO_2@AK branch were similar to those of SiO_2@AK and APTES@Kaolin and exhibited H3 type hysteresis loops with increasing pressure. Compared to SiO_2@AK, which retained a mesoporous structure, the pore sizes of 8-HQ@SiO_2@AK were slightly smaller, as shown in Fig. 6b and Table 1. This likely occurred because the small molecules of 8-HQ filled the surface micropores. The results of the SEM study were compatible with the 8-HQ@SiO_2@AK pore size distribution curves, specific surface area, and total pore volume, which did not differ significantly from those of

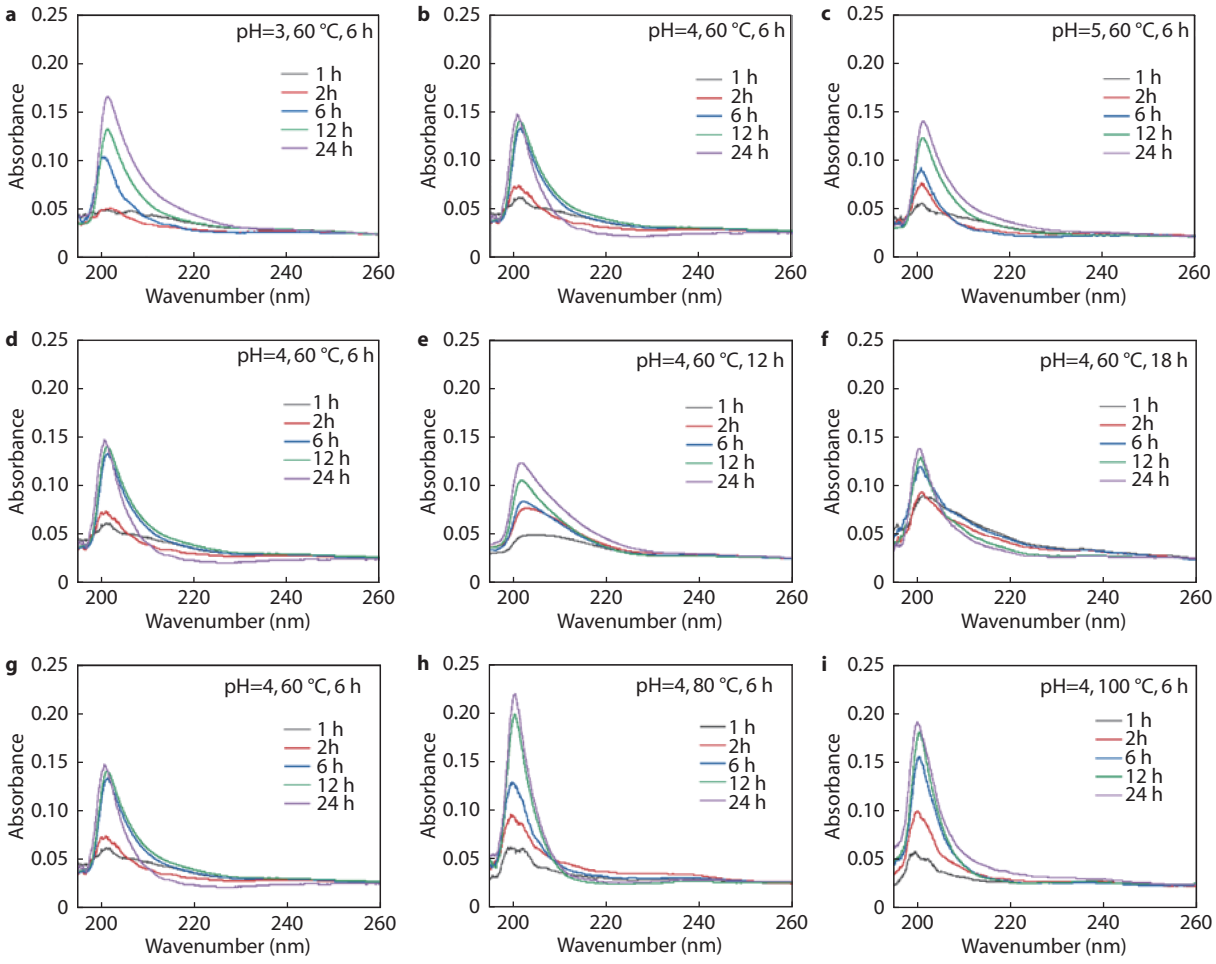


Fig. 3 UV diagrams of 8-HQ@SiO_2@AK prepared in different conditions: **a-c** different reaction pH; **d-f** different reaction time and **g-i** different reaction temperature.

DOI: 10.54227/mlab.20230018

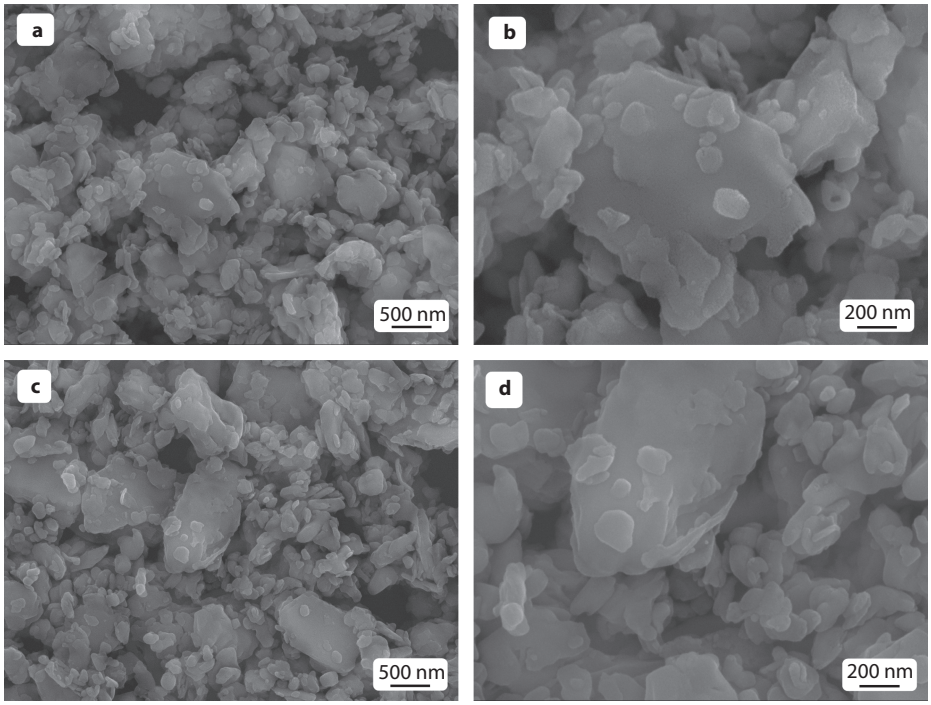


Fig. 4 SEM images of **a-b** SiO_2@AK and **c-d** 8-HQ@SiO_2@AK.

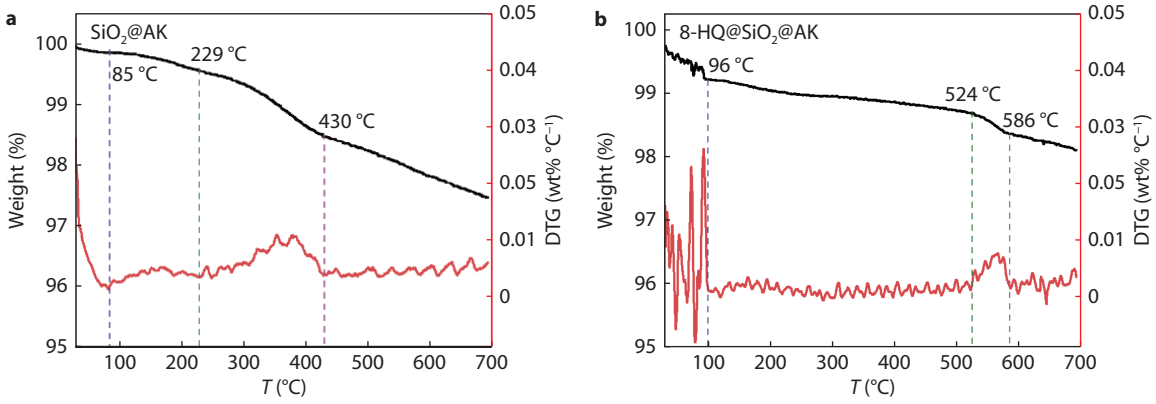


Fig. 5 TG and DTG curves of **a** SiO_2@AKand **b** 8-HQ@SiO_2@AK.

SiO_2@AK. This suggested that the composites retained their original structures.

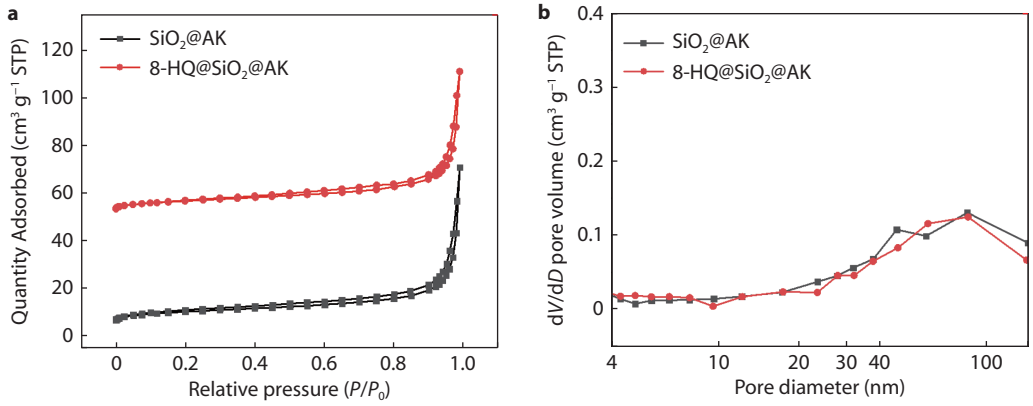


Fig. 6 N_2 adsorption and desorption isotherm of **a** 8-HQ@SiO_2@AK and **b** the corresponding pore size of materials.

DOI: 10.54227/mlab.20230018

Characterization and analysis of 8-HQ@SiO_2@AK/EP

Fig. 7 shows the water contact angle data for samples of the composite coating 8-HQ@SiO_2@AK/EP prepared under different conditions. Fig. 7a-d shows that the hydrophobicity of the composite coating slightly decreased after the introduction of the small molecule 8-HQ into SiO_2@AK, which may have been due to a reaction of the gel material on the surface of the 2D material under acidic conditions, exposure of the hydrophilic -OH groups inside the material and an increase in the number of hydroxyl radicals on the surface of the material, which are consistent with the FTIR data. Fig. 7b-d shows the hydrophobicities of composite coatings prepared with different reaction times, pH values and temperatures. The hydrophobicity of the 8-HQ@SiO_2@AK/EP decreased with increasing reaction time and temperature because longer reaction times and higher temperatures caused more decomposition of the gel material on the surface of the 2D material under acidic conditions, and more hydrophilic groups on the surface and inside of the material were exposed; however, changing the pH of the reaction solution had little effect on the hydrophobicities.

Fig. 8a-c shows the AFM 3D images for the APTES@Kaolin/EP, SiO_2@AK/EP and 8-HQ@SiO_2@AK/EP coatings, respectively, and Fig. 8d-f shows the corresponding 2D images. The surface roughnesses of the composite coatings were analysed by AFM, and the 2D and 3D plots showed that after loading the 8-HQ organic small molecules on the SiO_2@AK/EP, the surface micropores of the 8-HQ@SiO_2@AK/EP composite coatings were reduced and evenly distributed, while the surface defects of the SiO_2@AK/EP were larger and unevenly distributed due to reactions of the 2D material surface under acidic conditions. The reaction of the gel on the surface of the 2D material. As seen from Table 2, the root mean square roughness Rq and the mean surface roughness Ra of 8-HQ@SiO_2@AK/EP were slightly lower than those of SiO_2@AK/EP due to the 8-HQ loaded onto the reactive sites; this improved the compatibility between the composite and the epoxy resin, as suggested by the hydrophobicity analyses.

Fig. 9a-c shows the surface morphologies of the APTES@Kaolin/EP, SiO_2@AK/EP and 8-HQ@SiO_2@AK/EP composite coatings. The SEM images of 8-HQ@SiO_2@AK/EP showed a uniform distribution and less agglomeration of the composite material in the epoxy coating compared to that of SiO_2@AK/EP. Introduction of the small molecule corrosion inhibitor 8-HQ improved the compatibility of the composite with the epoxy coating and made the surface of the compos-

Table 1. N_2 isothermal adsorption and desorption test results of materials.

Compound Material	Average Pore Diameter (nm)	SSA ($m^2\ g^{-1}$)	Pore Volume ($cm^3\ g^{-1}$)
SiO_2@AK	24.63	16.32	0.1005
8-HQ@SiO_2@AK	22.28	16.31	0.0909

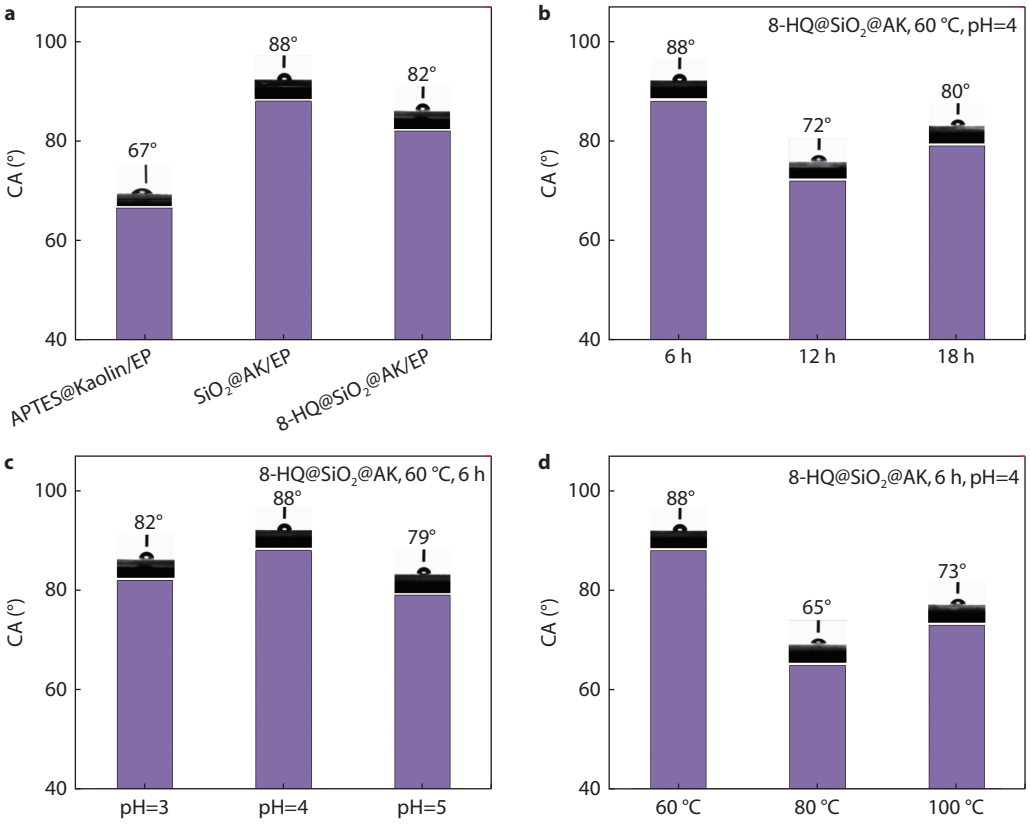


Fig. 7 Histograms of water contact angle test of SiO_2@AK/EP coatings in different reaction conditions: **a** the water contact angle before and after modification of composite coatings; **b** different reaction time; **c** different reaction pH and **d** different reaction temperature.

DOI: 10.54227/mlab.20230018

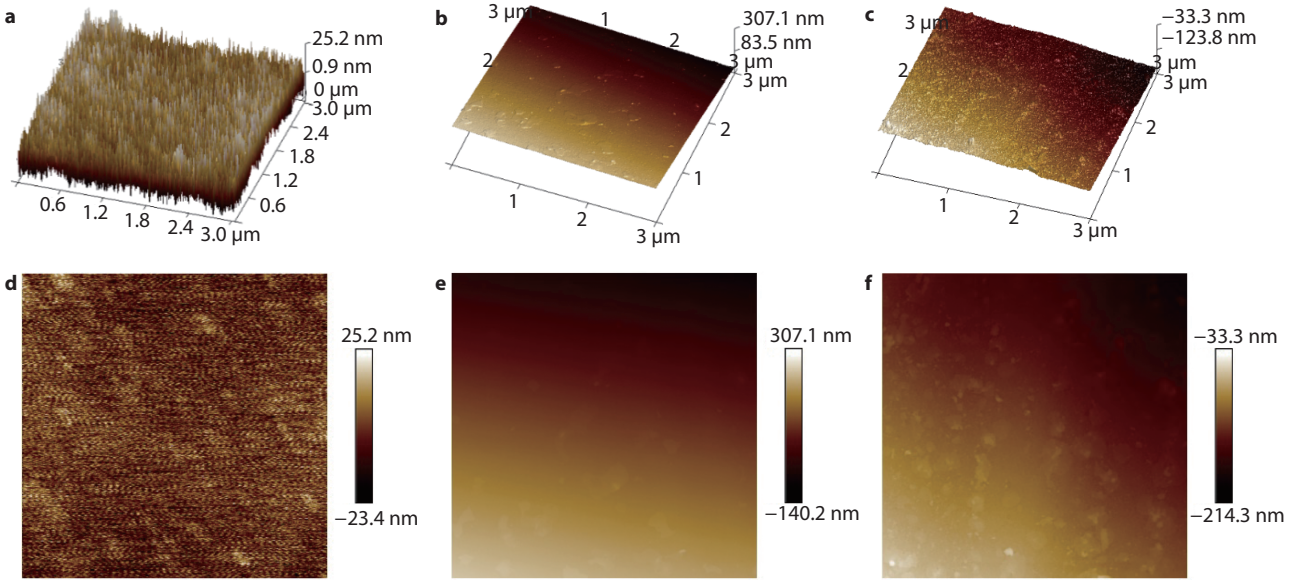


Fig. 8 The AFM images of **a** APTES@Kaolin/EP; **b** SiO_2@AK/EP and **c** 8-HQ@SiO_2@AK/EP coatings.

Table 2.

Composite Coating	RMS Rq (nm)	Average Roughness Ra (nm)
APTES@Kaolin/EP	7.04	5.64
SiO_2@AK/EP	3.89	3.19
8-HQ@SiO_2@AK/EP	3.70	3.09

ite coating smoother, which was consistent with the results of the AFM analysis.

8-HQ@SiO_2@AK/EP performance tests

Hardness testing of 8-HQ@SiO_2@AK/EP

Table 3 shows the hardness test results for the three composite coatings APTES@Kaolin/EP, SiO_2@AK/EP and 8-HQ@SiO_2@AK/EP. The test results showed that the 8-HQ@SiO_2@AK/EP composite coating had a rating of 6H, which indicated strong hardness.

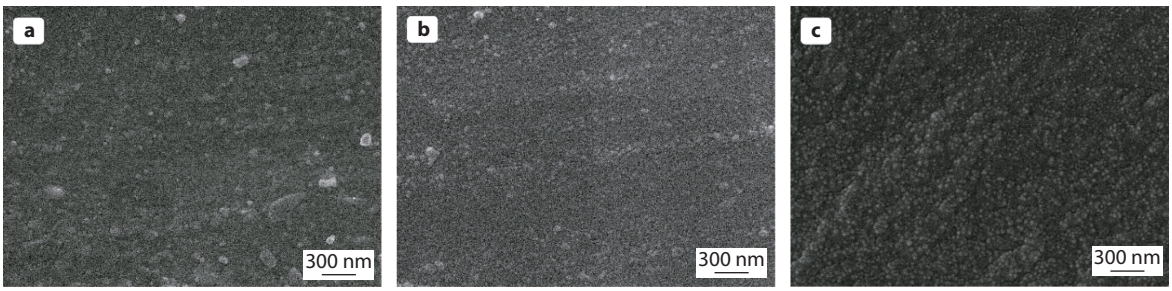


Fig. 9 The SEM images of **a** APTES@Kaolin/EP, **b** SiO_2@AK/EP and **c** 8-HQ@SiO_2@AK/EP coatings.

Table 3. The hardness test results of coatings.

Composite Coating	APTES@Kaolin/EP	AK@SiO_2/EP	8-HQ@SiO_2@AK/EP
Hardness Class	6H	6H	6H

Adhesion analysis of 8-HQ@SiO_2@AK/EP

Using the test method of the national standard GB/T9286-98, a paint film scribe was used to test the adhesion of the composite coatings separately. Fig. 10a-c shows the paint film scratch test data for the APTES@Kaolin/EP, SiO_2@AK/EP and 8-HQ@SiO_2@AK/EP composite coatings, respectively. The scratches were carefully observed at triple magnification, and all three composite coatings showed no peeling at the cut edges and adhesion test grades of 0. The experimental results showed that the introduction of the organic small molecule 8-HQ did not damage the bond between the composite coating and the substrate and that the 8-HQ@SiO_2@AK/EP coating still exhibited strong adhesion to the steel plate.

Scratch immersion testing of 8-HQ@SiO_2@AK/EP

Fig. 11a-c shows the scratch soak diagrams of the APTES@Kaolin/EP, SiO_2@AK/EP and 8-HQ@SiO_2@AK/EP coatings, respectively. To simulate the corrosion of the coating after the breakage in the service environment, the composite-coated steel plates were cut in an "X" pattern and immersed in a 3.5 mass% NaCl solution for 24 h. At the end of immer-

DOI: 10.54227/mlab.20230018

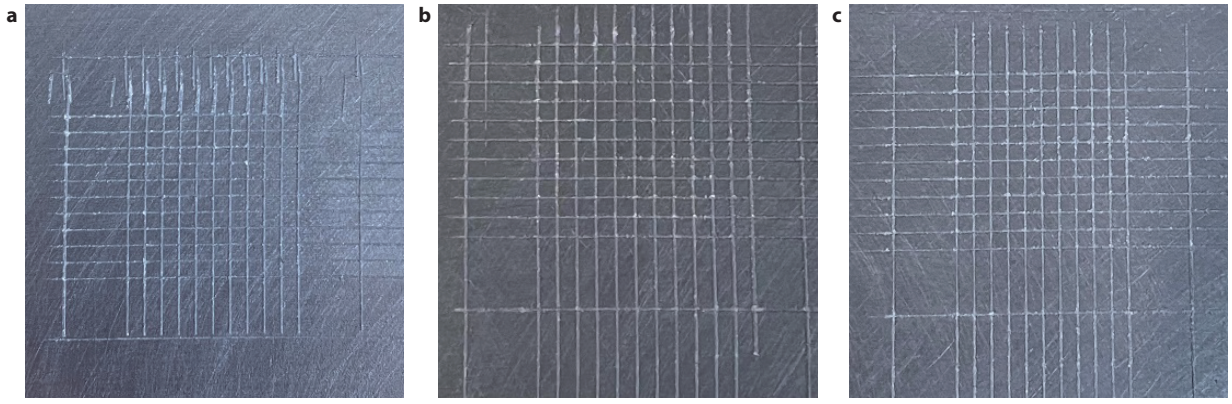


Fig. 10 Paint film cross-cut test pictures of **a** APTES@Kaolin/EP, **b** SiO_2@AK/EP and **c** 8-HQ@SiO_2@AK/EP coatings.

sion, the corrosion of the steel plates around the "X" was observed. After 24 h of immersion, the composite coatings SiO_2@AK/EP and 8-HQ@SiO_2@AK/EP showed no obvious corrosion, and the steel plate surfaces were in good condition. This showed that after introducing the organic small molecule 8-HQ into the epoxy resin, the composite coating maintained its good anti-corrosion properties, and the corrosion resistance of the composite coating was also tested with EIS.

AC impedance testing of 8-HQ@SiO_2@AK/EP

Fig. 12a-f shows Nyquist and Bode plots for the APTES@Kaolin/EP, SiO_2@AK/EP and 8-HQ@SiO_2@AK/EP composite coatings immersed in a 3.5 mass% NaCl solution for 2, 10 and 30 days, respectively. The graphs show that only a one-time constant was observed in the Nyquist and Bode plots for the different composite coatings immersed at different times, indicating that the composite coatings blocked the corrosive media over the 30-day immersion time. As the immersion time was increased, the tolerable arc radii of the coatings all showed gradual decreases. Compared with that for SiO_2@AK/EP, the radius of the permissive arc resistance for 8-HQ@SiO_2@AK/EP was significantly larger, indicating that the introduction of the 8-HQ corrosion inhibitor significantly improved the corrosion resistance of the composite coating. As seen from the Bode plot, the impedance modulus of the 8-HQ@SiO_2@AK/EP composite coating, $|Z|_{0.01Hz}$, was approximately $2.147 \times 10^{10}\ \Omega \cdot cm^2$, which was significantly higher than that of the SiO_2@AK/EP composite coating. After 30 days of immersion, the impedance modulus $|Z|_{0.01Hz}$ of 8-HQ@SiO_2@AK/EP was approximately $3.662 \times 10^9\ \Omega \cdot cm^2$, indicating that the small molecule corrosion inhibitor 8-HQ slowed the corrosion rate of the metal.

TUNEL test of 8-HQ@SiO_2@AK/EP

The polarization curves for the APTES@Kaolin/EP, SiO_2@AK/EP and 8-HQ@SiO_2@AK/EP coatings subjected to 30 days of immersion in a 3.5 mass% NaCl solution are shown in Fig. 13, and Table 4 shows the corrosion potentials (E_{corr}) and corrosion current densities (I_{corr}) for the composite coatings. As seen from the graph, the E_{corr} value of −2917 V for the 8-HQ@SiO_2@AK/EP composite coating was higher than the corrosion potentials of the APTES@Kaolin/EP and SiO_2@AK/EP coatings. The I_{corr} value of the 8-HQ@SiO_2@AK/EP composite coating was 1.060×10^{-13} A • cm^{-2}, which was slightly smaller than that of the SiO_2@AK/EP composite coating. The higher E_{corr} and lower I_{corr} values indicated a higher corrosion resistance for the coating. The results showed that the introduction of the small molecule corrosion inhibitor 8-HQ inhibited corrosion and thus improved the corrosion protection of the composite coating.

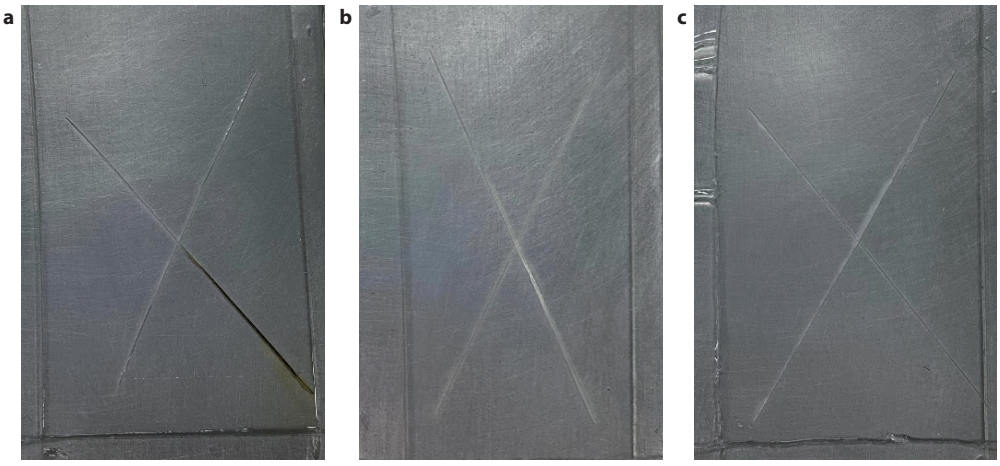


Fig. 11 Scratch immersion test images of **a** APTES@Kaolin/EP, **b** SiO_2@AK/EP and **c** 8-HQ@SiO_2@AK/EP coatings.

DOI: 10.54227/mlab.20230018

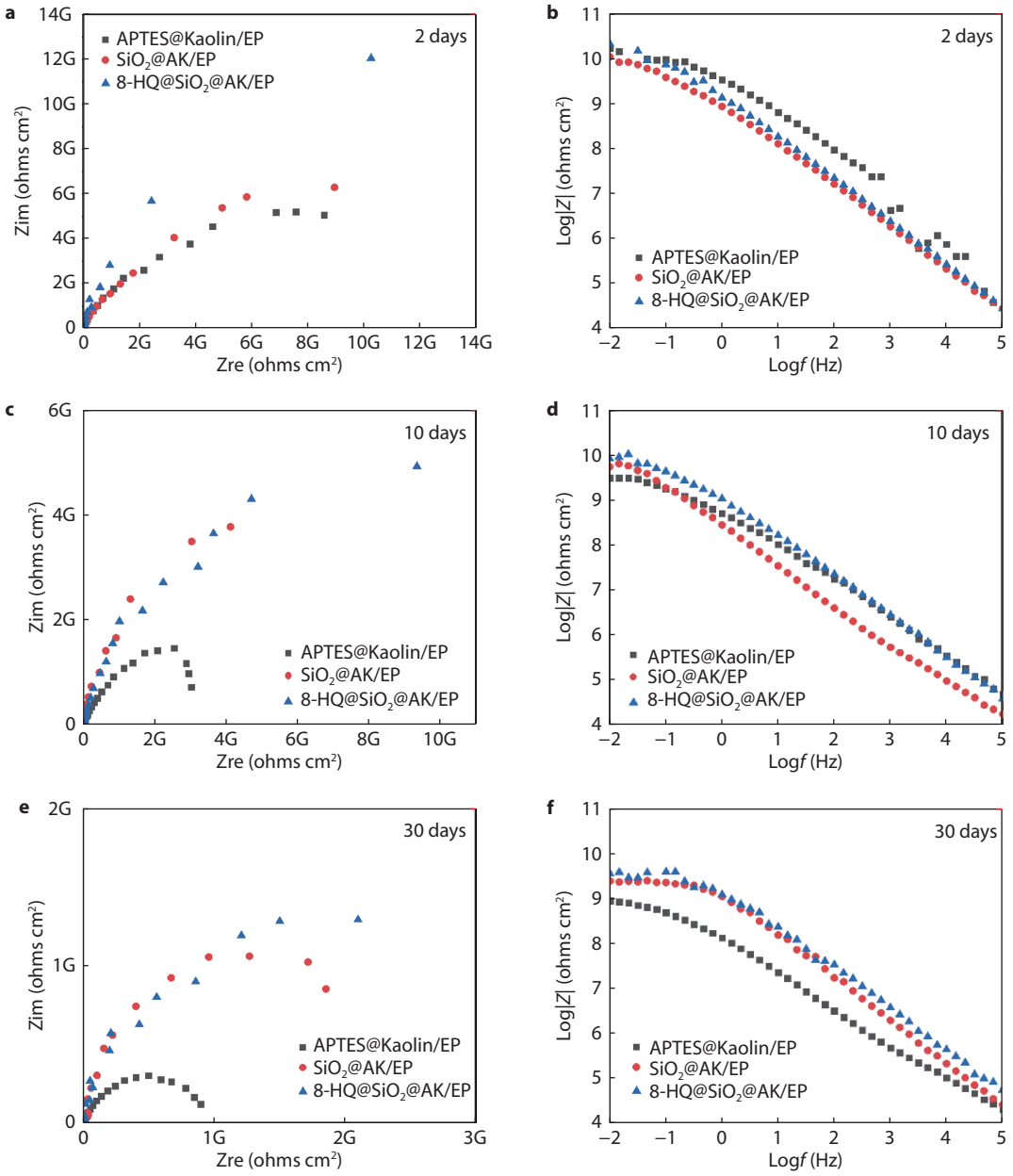


Fig. 12 The Nyquist and Bode diagrams of 8-HQ@SiO_2@AK/EP coating immersing in 3.5% NaCl solution for **a-b** 2 days, **c-d** 10 days and **e-f** 30 days.

Conclusions

In this study, SiO_2@AK and the small molecule corrosion inhibitor 8-HQ were used as raw materials to prepare the composite 8-HQ@SiO_2@AK via a hydrothermal reaction run under an acidic environment for inorganic particle modification. The composite coating 8-HQ@SiO_2@AK/EP was prepared by adding the composite as a filler into the epoxy resin. The morphologies, hydrophobicities, surface roughnesses and electrochemical properties of the composite coatings were also investigated, and the following conclusions were drawn.

(1) The composites were analysed by FTIR, XRD and TGA, and the results showed that 8-HQ was successfully loaded into SiO_2@AK with few changes in the structures of the composites.

(2) Due to the entry of small molecules 8-HQ into the pores on the material surface, the average pore size of the composite material decreased from 24.63nm to 22.28nm. The total pore volume and specific surface area did not show significant changes, indicating that the composite material structure was maintained. And at a pH of 3, a reaction temperature of 60 °C, and a reaction time of 7 hours, the maximum loading capacity of 8-HQ was reached.

(3) The tests of hydrophobicity, hardness and adhesion showed that the hydrophobicity of 8-HQ@SiO_2@AK/EP was lower than that of SiO_2@AK/EP due to decomposition of the 2D surface material under acidic conditions and exposure of the hydrophilic groups. After 30 days of immersion, the impedance modulus$|Z|_{0.01Hz}$ was 3.662×10^9 Ω·cm², indicating that the composite coating 8-HQ@SiO_2@AK/EP provided the

DOI: 10.54227/mlab.20230018

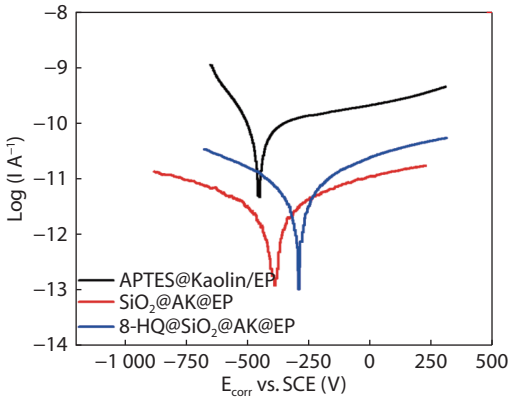


Fig. 13 Polarization curves of APTES@Kaolin/EP, SiO_2@AK/EP and 8-HQ@SiO_2@AK/EP coatings immersed in 3.5% NaCl solution for 30 days.

Table 4.

Composite Coating	E_{corr} (V)	I_{corr} (A cm^{-2})
APTES@Kaolin/EP	−0.4509	4.785×10^{-12}
SiO_2@AK/EP	−0.3911	1.230×10^{-13}
8-HQ@SiO_2@AK/EP	−0.2917	1.060×10^{-13}

best corrosion protection.

Acknowledgements

This work was partially supported by grants from Natural Science Foundation of Henan Province (212300410082) and Project funding for Young Backbone Teachers in Colleges and Universities of Henan Province (2020GGJS013). These grants are gratefully acknowledged.

Conflict of interest

The authors declare that they have no known competing financial interests or personal relationships that could have appeared to influence the work reported in this paper.

■ REFERENCES

1. B. Ehsan, J. Ali, R. Zahra, S. Sarah, S. Mohammad Reza, *Progress in Organic Coatings*, 2014, 77, 1169
2. K. Chang, M. Hsu, H. Lu, M. Lai, P. Liu, C. Hsu, W. Ji, T. Chuang, Y. Wei, J. Yeh, W. Liu, *Carbon*, 2014, 66, 144
3. L. Neill, S. Gin, T. Ducasse, T. D. Echave, M. Fournier, P. Jollivet, A. Gourgiotis, N. A. Wall, *NPJ Materials Degradation*, 2017, 1, 1
4. I. Lanneluc, M. Langumier, R. Sabot, M. Jeannin, P. Refait, S. Sablé, *International Biodeterioration & Biodegradation*, 2015, 99, 55
5. S. K. Dhaliwal, B. P. Meek, M. M. Modirrousta, *Frontiers in Psychiatry*, 2015, 6, 7
6. B. Zhang, J. Li, X. Zhao, X. Hu, L. Yang, N. Wang, Y. Li, B. Hou, *Chemical Engineering Journal*, 2016, 306, 441
7. X. Wei, C. Ning, Z. Lu, J. Zhang, *Ceramics International*, 2022, 48, 8440
8. M. D. Maksimović, V. B. Mišković-Stanković, *Corrosion Science*, 1992, 33, 271
9. H. Bi, J. Sykes, *Progress in Organic Coatings*, 2015, 87, 83
10. M. Sababi, H. Terryn, J. M. C. Mol, *Progress in Organic Coatings*, 2017, 105, 29
11. M. M. Tabatabaei, D. Mahsa, R. Mohammad, G. Ebrahim, R. Bahram, M. Mohammad, *Construction and Building Materials*, 2020, 247, 118555
12. F. Meng, L. Liu, W. Tian, H. Wu, Y. Li, T. Zhang, F. Wang, *Corrosion Science*, 2015, 101, 139
13. R. Shamim, D. A. Asghar Sarabi, M. Javad, *Applied Surface Science*, 2018, 440, 880
14. M. Tamilselvi, P. Kamaraj, M. Arthanareeswari, S. Devikala, J. Selvi, *Applied Surface Science*, 2015, 332, 12
15. A. Ghanbari, M. M. Attar, *Journal of Industrial & Engineering Chemistry*, 2015, 23, 145
16. S. S. Golru, M. M. Attar, B. Ramezanzadeh, *Progress in Organic Coatings*, 2014, 77, 1391
17. L. Liu, J. Xu, *Vacuum*, 2011, 85, 687
18. B. Ramezanzadeh, M. M. Attar, M. Farzam, *Progress in Organic Coatings*, 2011, 72, 410
19. T. A. Truc, T. T. Thuy, V. K. Oanh, T. T. X. Hang, A. S. Nguyen, N. Causse, N. Pebere, *Surfaces and Interfaces*, 2019, 14, 26
20. K. Zhang, L. Wang, G. Liu, *Corrosion Science*, 2013, 75, 38
21. F. Sara, P. Massimo, P. Giovanni, N. T. Dintcheva, M. Pierluigi, *Polymer Degradation and Stability*, 2011, 96, 823

©2024 The Authors. *Materials Lab* is published by Lab Academic Press. This is an open access article under the terms of the Creative Commons Attribution License, which permits use, distribution and reproduction in any medium, provided the original work is properly cited.